

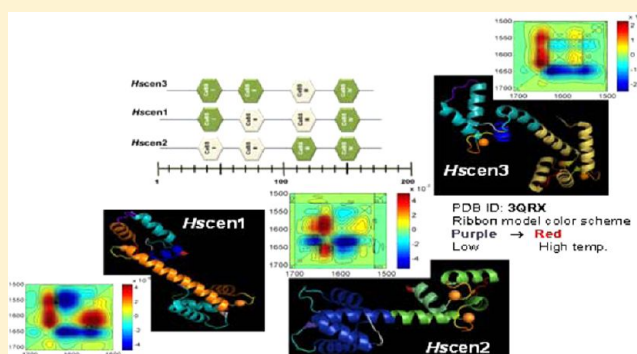
Relative Stability of Human Centrins and Its Relationship to Calcium Binding

Belinda Pastrana-Ríos,^{*,†,‡} Myrna Reyes,[‡] Jessica De Orbeta,[‡] Verónica Meza,[‡] Daniel Narváez,[‡] Ana María Gómez,[‡] Aslin Rodríguez Nassif,[‡] Ruth Almodovar,[‡] Adalberto Díaz Casas,[‡] José Robles,[‡] Ana María Ortiz,[‡] Lizbeth Irizarry,[‡] Melissa Campbell,[‡] and Mara Colón[‡]

[†]Protein Research Center and [‡]Department of Chemistry, University of Puerto Rico, Mayagüez Campus, Mayagüez, Puerto Rico 00681-9019, United States

S Supporting Information

ABSTRACT: Centrins are calcium binding proteins that belong to the EF-hand superfamily with diverse biological functions. Herein we present the first systematic study that establishes the relative stability of related centrins via complementary biophysical techniques. Our results define the stepwise molecular behavior of human centrins by two-dimensional infrared (2D IR) correlation spectroscopy, the change in heat capacity and enthalpy of denaturation by differential scanning calorimetry, and the relative stability of the helical regions of centrins by circular dichroism. More importantly, 2D IR correlation spectroscopy provides unique information about the similarities and differences in dynamics between these related proteins. The thermally induced molecular behavior of human centrins can be used to predict biological target interactions that have a relative dependence on calcium affinity. This information is essential for understanding why certain isoforms may be used to rescue a phenotype and therefore also for explaining the different functions these proteins may have in vivo. Furthermore, this comparative approach can be applied to the study of recombinant therapeutic protein candidates for the treatment of disease states.



Centrin is one of 350 eukaryotic signature proteins thought to be critical to the structure and function of the eukaryotic cell.^{1,2} In higher eukaryotes, e.g., *Homo sapiens*, there are four centrin isoforms: centrin 1, centrin 2, centrin 3, and the pseudogene centrin 4 (abbreviated as *Hscen1*–*Hscen4*, respectively). These centrins are localized to different cellular compartments or associated with specialized tissues with different biological functions, yet in other eukaryotes, only one centrin is required.³ All four isoforms have been associated with the interconnecting cilia within the retina and have been associated with visual signal transduction.⁴ *Hscen4* has also been found in neuronal cells within the brain, while *Hscen3* has been localized to the distal lumen of the centrioles and basal bodies.^{4,5} *Hscen2* has been found to regulate DNA excision repair within the nucleus^{6,7} and export of mRNA from the nucleus.⁸ Finally, *Hscen1* is localized to the base of the flagella in the sperm and, by contributing the mother centriole of the sperm to the ovum to allow for centriole duplication, is therefore associated with the first division of the zygote.^{9,10}

The canonical role of centrin, and particularly *Hscen2*, is as a structural and regulatory component of the centriole and basal bodies,¹¹ such that it has commonly been used to identify centrioles and basal bodies in situ.¹² The assembly of the microtubule organizing center (MTOC), which includes centrioles and basal bodies, requires many of the same proteins

and is highly conserved in eukaryotes.^{11,12} Failure to duplicate the centriole properly once every cell cycle has been linked to hypertrophy of the centrosomes, aberrant chromosome segregation, and chromosome instability, all important factors in understanding cancer.^{13–15} Basal bodies are also associated with the assembly of cilia.¹⁶ There are two classes of cilia: the motile and the immotile, or primary cilia.^{16,17} Defects in the basal body are also associated with the aberrant assembly of primary cilia in higher eukaryotes.^{18,19}

Primary cilia, which are immotile and found in almost all organs of the human body, act as a sensory receptor for the cell.^{18,20} If the primary cilia are found to be defective, their photo-, chemo-, and mechanosensory roles will also be defective. A defective ciliary structure has been recently associated with ciliopathy.

Ciliopathies are a new clinical classification of an expanding group of genetic disorders that cause ciliary dysfunction in many organs.^{18–23} They include polycystic kidney disease, nephronophthisis, retinal degeneration, such as retinitis pigmentosa, and a series of cilia-associated syndromes such as Bardel-Biedl, Joubert, Alström, and Meckel syndrome, among

Received: October 17, 2012

Revised: January 20, 2013

Published: January 24, 2013

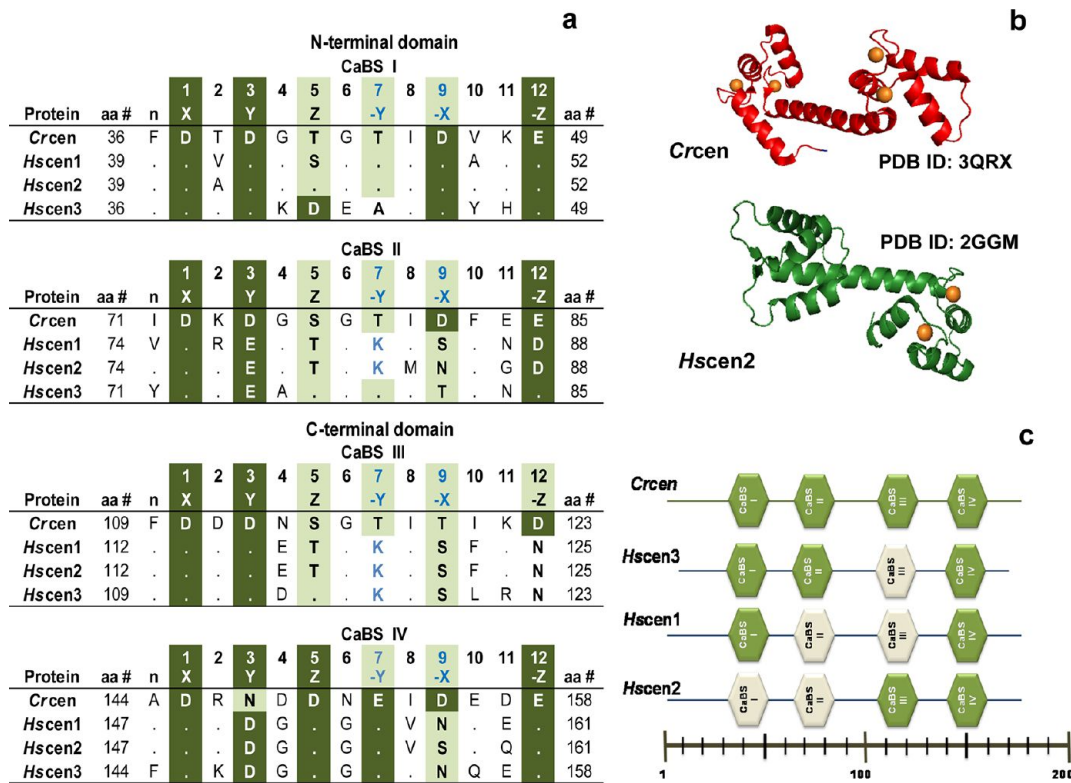


Figure 1. EF-hand calcium binding sites (CaBS). (a) Sequence alignment based on the following NCBI accession numbers: XP_001699499 (*Crcen*), EAX01727 (*Hscen1*), EAW72900 (*Hscen2*), and AAI12041 (*Hscen3*).^{30–32} Dots in the CaBS sequence alignment represent identical residues when compared to the first sequence (*Crcen*). (b) Ribbon models of the available full-length *Crcen* (red ribbon) and *Hscen2* (green ribbon) structures were generated from Protein Data Bank entries 3QRX and 2GGM, respectively, using pyMOL from Schrödinger, LLC.^{35,36} Ca²⁺ is represented as orange spheres. (c) Schematic diagram of the predicted low-affinity (white) and high-affinity (green) CaBS based on the sequence analysis. In *Crcen*, the N-terminal domain is composed of high-affinity CaBS as compared to the C-terminal domain, which has the low-affinity sites, yet all sites bind calcium.^{35,36} *Hscen3*'s CaBS III is predicted to have a low affinity for Ca²⁺ because of the presence of aspartate residues at positions 2 and 4, which are generally associated with decreased calcium affinity.³² Similarly, for *Hscen1* and *Hscen2*, the presence of the aspartate or asparagine residue at position 12 in CaBS II and III is also predictive of low calcium affinity because of the lack of bidentate coordination with calcium.^{32,36,37} Finally, residues found in the N-terminal end (as shown in Figure 2) may influence the calcium affinity of the the first CaBS in *Hscen2*, specifically Asn₉, when compared to Ser₉ of *Hscen1*.

others.^{19–26} These syndromes are usually observed within family members with different clinical symptoms or phenotypes. The extent of the clinical variability in the phenotypes even within the same family cannot be explained solely on a genetic basis (single-locus allelism).^{19,21,24–26} Therefore, an alternate mechanism must also be involved to explain the variability in phenotype. One possible explanation for the observed variability in ciliopathy phenotypes may be the variable expression of conserved proteins^{27,28} or variability in the function of calcium binding proteins.²⁹

Hscen1–Hscen3 are calcium binding proteins that share common biochemical and structural properties with each other and with *Chlamydomonas reinhardtii* centrin (*Crcen*). Their molecular mass is ~20 kDa; their sequences are >52% identical (Figure S1 of the Supporting Information), and they have an acidic isoelectric point.^{30,31} Upon closer examination, the sequence of *Crcen* is >71% identical with those of *Hscen1* and *Hscen2*, while for *Hscen3*, the level of sequence identity is 52%; the level of sequence identity between *Hscen1* and *Hscen2* is 84%. Like other EF-hand proteins, centrans respond to cellular Ca²⁺ influx by selectively binding Ca²⁺ ions in highly conserved helix–loop–helix motifs.^{30–35} EF-hand proteins have two globular domains linked by a tethered helix (Figure 1). Each globular domain is composed of two helix–loop–helix motifs,

each capable of binding calcium. It is within the loop region that five of six Ca²⁺-binding residues coordinate directly with a divalent cation. The geometry adopted for calcium binding is that of a pentagonal bipyramid, which can be described in a Cartesian coordinate system as X, Y, Z, –X, –Y, and –Z. The X, Y, Z, and –Z positions coordinate calcium through Asp[–] or Glu[–] carboxylates; in the –Y position, the coordination occurs via a backbone carbonyl group, and in the –X position, the residue coordinates indirectly through a water molecule. In canonical EF-hand proteins, like *Crcen*, there are two high-affinity sites and two low-affinity sites for calcium, as shown in Figure 1. The dissociation constants range from 1 nM to 0.1 mM. However, *Hscen1* and *Hscen2* calcium binding sites (CaBS) II and III have a sequence that contributes to lower affinity, with Asp₈₈ or Asn₁₂₅ being responsible for the bidentate coordination of Ca²⁺ at the –Z (12) position^{30–33} (Figure 1a).

While human centrans share similar biochemical and structural properties, a gap exists in our understanding of the relationship between their structure and the diversity of their biological roles. Herein, we present for the first time a comparative molecular biophysical study involving differential scanning calorimetry (DSC),³⁶ circular dichroism (CD),³⁷ and two-dimensional infrared (2D IR) correlation spectroscopy^{38–42} to assess the relative stability of related centrin proteins

that establishes the differences in molecular flexibility and dynamics as a function of temperature. These novel 2D IR correlation spectroscopic results provide unique insight into the molecular behavior these proteins exhibit as a function of temperature, while relating these differences to their lower- and higher-calcium affinity sites. These factors may be crucial in determining their different biological roles and potentially may provide new insight into the modulation of their binding affinities and the role of the EF-hand motif in the regulation of centrin–target interactions.

■ EXPERIMENTAL PROCEDURES

Bacterial Expression. The *Hscen1* and *Hscen2* cDNA inserts were generously supplied by E. Schiebel (Peterson Institute for Cancer Research, Manchester, United Kingdom), while the *Hscen3* clone was generously supplied by J. Kilmartin (University of Cambridge, Cambridge, United Kingdom). These cDNA inserts were subcloned into a pT7-7 expression vector and transformed into *Escherichia coli* BL21(λ DE3) Star from Stratagene. The new recombinants were then sequenced to verify the identity, proper orientation, and reading frame by J. C. Martinez-Cruzado (University of Puerto Rico, Mayagüez, PR).

The fed-batch method was employed for a 5 L BIOFLO 3000 fermentor (New Brunswick Scientific, Edison, NJ) of *E. coli* BL21(λ DE3) Star cells newly transformed with the desired recombinant. The bacterial cultures were grown in terrific broth medium (Bio 101, Inc., Carlsbad, CA) at 37 °C with 350 rpm agitation, while the dissolved oxygen, pH, and cell density were monitored. Bacterial cultures were induced with 0.5 mM isopropyl β -D-thiogalactoside at the onset of the log phase. Cells were harvested by centrifugation once the stationary phase was reached, usually 3–4 h after induction. Typical yields were 40–80 g of pelleted cells from a 4 L culture.

Isolation and Purification. The purification protocols have all been established in our laboratory.^{32,40,42} The isolation protocol has been modified to improve the subsequent purification process. Routinely, the harvested cell pellet was lysed using a cold buffer solution containing 50 mM Tris, 0.5 mM EDTA, 0.5 M NaCl, 0.04% NaN₃, and 1% IGEPAL (pH 7.4). To minimize proteolytic cleavage of the desired recombinant protein, a cocktail of protease inhibitors was also added (2.0 mg/mL aprotinin, 0.5 mg/mL leupeptin, 1.0 mg/mL pepstatin A, and 2 μ L/mL crude lysate of Pefabloc SC). The crude lysate was subjected to preparative centrifugation using a JA-14 rotor and a Beckman J2-MC centrifuge at 9615g for 15 min at 4 °C. This first supernatant sample was then ultracentrifuged using a TI-70 rotor and a Beckman L-80 ultracentrifuge at 70588g for 30 min at 4 °C. This second supernatant was then incubated at 60 °C for 30 min followed by a final preparative centrifugation to remove denatured host protein precipitate using a JA-14 rotor and a Beckman J2-MC centrifuge at 3840g for 30 min at 4 °C to recover the third and final supernatant. This final supernatant sample was then clarified using a hollow fiber cartridge with a 0.1 μ m cutoff membrane. The clarified sample was then subjected to buffer exchange using tangential flow filtration with a 5 kDa membrane from Pall Corp. (Ann Arbor, MI). For purification, this sample was then applied to a Phenyl Sepharose CL4B affinity column and, if necessary, an anion exchange chromatography column. In each case, the eluted fractions were analyzed by sodium dodecyl sulfate–polyacrylamide gel electrophoresis (SDS–PAGE) and fractions containing the

desired centrin protein were pooled. Typically, 125–600 mg of >98% pure centrin protein was obtained from each batch.

Protein Sample Preparation. For each of the molecular biophysical methods performed below, the buffer conditions and protein concentration were identical to allow for comparative analysis. This was achieved by accurate concentration determination using the predicted molar extinction coefficients: $\epsilon_{280} = 1490 \text{ M}^{-1} \text{ cm}^{-1}$ for *Crcen*, *Hscen1*, and *Hscen2*, and $\epsilon_{280} = 8480 \text{ M}^{-1} \text{ cm}^{-1}$ for *Hscen3*. Direct UV absorbance measurements were taken only after exhaustive dialysis of the desired protein against the appropriate buffer conditions using a 5 kDa membrane.

Differential Scanning Calorimetry. Routinely, the desired centrin (1.0 mg/mL) in 50 mM HEPES, 150 mM NaCl, 4 mM CaCl₂, and 4 mM MgCl₂ (pH 7.4) was analyzed with a VP-DSC microcalorimeter from MicroCal LLC (Northampton, MA). Thermograms were collected at 25 psi and a scan rate of 60 °C/h over a temperature range of 10–127 °C, with an 8 s filtering period. The data analysis was performed using Origin from MicroCal. The sample thermograms were reference subtracted, normalized for concentration to determine the change in heat capacity (ΔC_p), and a progressive baseline was obtained to allow for accurate determination of the change in the enthalpy of denaturation (ΔH_D) and T_m .^{36,43}

Circular Dichroism. Centrin samples (2.3 μ M) in 8 mM HEPES, 2 mM CaCl₂, 2 mM MgCl₂, and 50 mM NaCl (pH 7.4) were used to acquire far-UV CD spectra on a Jasco (Tokyo, Japan) model J-810 spectropolarimeter equipped with a Peltier temperature controller accessory. The instrument was calibrated using (+)-10-camphorsulfonic acid. Five scans, within the spectral range of 250–190 nm, were collected at a scan rate of 20 nm/min at 5, 25, and 85 °C. In addition, temperature dependence spectra were also collected from 0 to 95 °C, while being monitored at 222 nm at a rate of 1 °C/min. The CD absorbance was converted to mean residue molar ellipticity for each spectral data set to allow for proper comparison between the centrin proteins.^{37,44} Origin 7 professional software from MicroCal was used to render the desired plots.

Vibrational Spectroscopy. The protein samples were dialyzed under the desired buffer conditions and then lyophilized repeatedly to H \rightarrow D exchange the sample as previously described.^{32,40–42} A 35 μ L aliquot of 60 mg/mL protein in 50 mM HEPES, 150 mM NaCl, 4 mM MgCl₂, and 4 mM CaCl₂ (pD 6.6) was deposited on a 49 mm \times 4 mm custom-milled CaF₂ window with a fixed path length of 40 μ m. A reference cell was prepared similarly, and both cells were set in a custom dual-chamber cell holder. The temperature within the cell was controlled via a Neslab RTE-740 refrigerated bath (Thermo Electron Corp.) and monitored with a thermocouple positioned in close contact with the sample cell. The accuracy of the temperature was estimated to be within ± 1 °C. Routinely, spectral data acquisition was performed at the desired preset temperature with 10 min intervals, once the temperature in the cell was reached, to allow for thermal equilibrium of the sample. A Jasco model 6200 FT-IR spectrophotometer equipped with a narrowband MCT detector, a sample shuttle, and an interface was used. Typically, 512 scans were co-added, apodized with a triangular function, and Fourier transformed to provide a resolution of 4 cm^{-1} with the data encoded every 2 cm^{-1} .

FT-IR Spectroscopy. This process provides information regarding the conformational dynamics of proteins. In

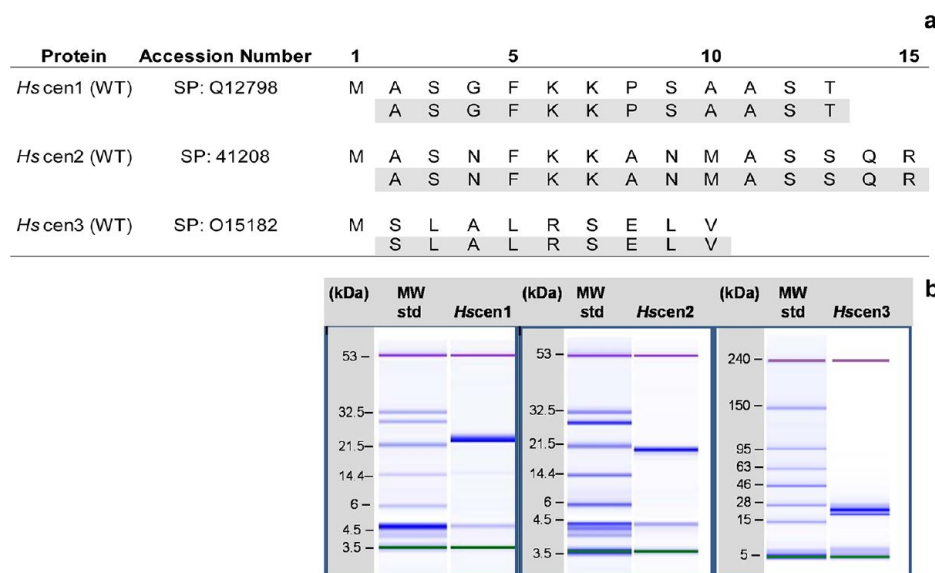


Figure 2. Biochemical characterization of *H. sapiens* centrin. (a) Partial amino acid sequencing analysis of the N-terminal end of the recombinant human centrin, validating their identity and the loss of M₁. (b) SDS-PAGE microchip analysis of the purified proteins. Each sample contained two internal standards to calibrate the relative mobility in each lane, with an associated band at 4.5 kDa that is also observed in the molecular mass standards. For the assays involving *Hscen1* and *Hscen2*, the lower internal standard was 3.5 kDa and the higher internal standard 53 kDa, while for *Hscen3*, the assay contained 5 and 240 kDa molecular mass internal standards. In each case, a single band was observed near the expected molecular mass.

particular, the amide I' band typically observed within the range of 1700–1600 cm⁻¹ is characteristic of peptide bonds within a protein, composed mainly of highly coupled carbonyl stretching modes [$\nu(\text{C}=\text{O})$] that are sensitive to the conformation of the protein. H → D exchange simplifies the underlying spectral contributions within the amide I', side chain, and amide II' bands as follows. As a result, the amide II band observed within the range of 1600–1500 cm⁻¹ is composed of the side chain modes. The amide N–H deformation modes of the peptide bonds within the amide II band (1550 cm⁻¹) shift ~100 cm⁻¹ to lower wavenumbers, to the amide II' band (1450 cm⁻¹). The protein sample is considered to be fully exchanged when reversibility is observed upon cooling after heating the amide I' band returns to the same position and intensity value when compared to the same temperature value upon heating. Therefore, the H → D exchange effectively reduces the number of contributing vibrational modes, without sacrificing structural and dynamic information about the behavior of the protein.^{32,40–42,45–50}

For the FT-IR spectral analysis, the spectral data were not manipulated except for baseline correction. The thermal dependence plots were generated using Origin version 7 from OriginLab Corp. (Northampton, MA).

2D IR Correlation Spectroscopy. Noda developed this technique.^{38,39} It uses the FT-IR series of sequential spectra as a function of a perturbation (temperature, H → D exchange, ligand titration, etc.) to generate synchronous and asynchronous plots. The spectra are collected at regular intervals of the perturbation. In general, the analysis spreads the acquired spectral data into two dimensions, thus enhancing the spectral resolution in the synchronous plot and providing information about the sequence of molecular events that occur in the asynchronous plot.^{32,38–42} Both plots provide information about the coupling of vibrational modes within the spectral region of interest (1710–1500 cm⁻¹). Consequently, this technique is sensitive to backbone vibrational modes as well as

certain side chain modes (i.e., arginine, aspartates, glutamates, and tyrosine) being perturbed, and as a result, one can identify changes in these modes as a function of the perturbation.

The spectral overlay, peak pick routines, and 2D IR correlation analysis were performed using a Kinetics program for MATLAB (MathWorks, Natick, MA) generously provided by E. Goormaghtigh (Free University of Brussels, Brussels, Belgium).

RESULTS

Partial Amino Acid Sequencing Results for *H. sapiens* Centrin. Figure 2 shows these results for all three isoforms. The expected amino acid sequence with the observed loss of the first methionine residue at the amino-terminal end verifies their identities. Also shown are the microchip SDS-PAGE analyses of the purified proteins for all three isoforms. In each case, a single band was observed, indicating >98% purity.

Thermal Denaturation of Centrin. The thermal unfolding process for these proteins was determined to be endothermic in each case by DSC, the results of which are summarized in Table 1, Figure 3, and Figure S2 of the Supporting Information. The relative stability of human centrin was compared to that of Crcen in which all CaBS

Table 1. Summary of the DSC Comparative Analysis of *H. sapiens* and *C. reinhardtii* Centrin

protein ^a	T _m ^b (°C)	ΔC _{pD} ^c (kcal mol ⁻¹ °C ⁻¹)	ΔH _D ^d (kcal/mol)	temperature range (°C)
<i>Hscen1</i>	89.52	0.4	17.9	65.06–126.26
<i>Hscen2</i>	81.90	0.3	40.0	55.01–115.09
<i>Hscen3</i>	95.72	–0.4	47.3	75.11–125.02
Crcen	111.32	0.2	93.5	85.11–126.40

^aWild-type recombinant proteins. ^bTransition temperature. ^cChange in the heat capacity of denaturation. ^dChange in the enthalpy of denaturation.

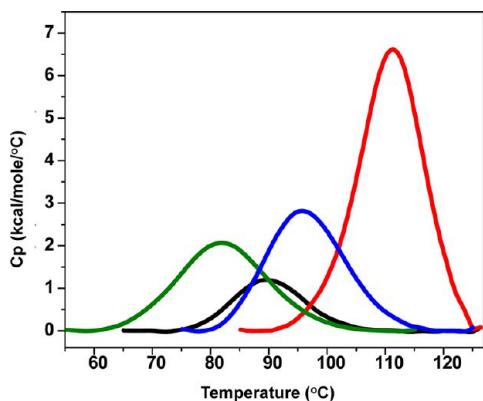


Figure 3. Overlay of DSC thermograms establishing the relative stability of *H. sapiens* and *C. reinhardtii* centrins: Hscen1 (black), Hscen2 (green), Hscen3 (blue), and Crcen (red). Their respective T_m values are 89.52, 81.90, 95.72, and 111.32 °C, respectively.

are occupied (Figure 1).^{32,42} There are two potential causes for the differences in stability. The first is the differences in calcium affinity, and the second is the sequence divergence of these proteins. The comparatively large differences in the T_m and the changes in the enthalpy of denaturation observed in our DSC analysis suggest that calcium affinity is the primary driver of the observed differences in the centrins' relative stability (results not shown). Crcen was determined to have the highest thermal transition temperature [111.32 °C (Table 1)], whereas Hscen3 was the most stable of the *H. sapiens* centrins. Hscen3's T_m was lower by 15.6 °C than that of Crcen, suggesting this is due to the lower calcium affinity as summarized in Figure 1. Similarly, for Hscen1 and Hscen2, whose calcium affinity differs even more from that of Crcen, the transition temperatures were 21.8

and 29.4 °C lower, respectively. The difference in T_m between Hscen1 and Hscen2, which have sequences that are >80% identical, was ~7.6 °C, suggesting that the differences in the transition temperature may be associated with changes in calcium binding as the EF-hand motif adopts different conformations in the presence (open conformation) and absence (closed conformation) of calcium.^{30,43} These two isoforms contain two lower-affinity CaBS (CaBS II and III for Hscen1 and CaBS I and II for Hscen2) located in the N- and C-terminal domains for Hscen1, while for Hscen2, the lower-affinity CaBS are located within the N-terminal domain.³¹ These lower-affinity sites could also account for the pretransitions observed within centrins (Figure S2 of the Supporting Information). As a result, differences in stability could also be translated into differences in backbone flexibility upon the transition between the open and closed conformations.

We also evaluated the change in the heat capacity of denaturation (ΔC_{pD}) and the change in the enthalpy of denaturation (ΔH_D) for these centrins, which provide additional insight into the differences in their stability (Table 1). For Hscen3, the ΔC_{pD} was negative, while for Crcen, Hscen1, and Hscen2, this value was positive, suggesting differences in side chain hydration contributions. Hscen3 contains a primarily nonpolar N-terminal end sequence (Figure 2), as well as a tryptophan residue and an additional tyrosine residue that are not present in the Hscen1 and Hscen2 sequences. More importantly, the lower ΔH_D of Hscen1 compared to that of Hscen2 is consistent with loss of calcium coordination at CaBS III because of the differences in calcium binding affinity observed for these two highly conserved proteins, as discussed below in 2D IR Correlation Spectroscopy. The concomitant

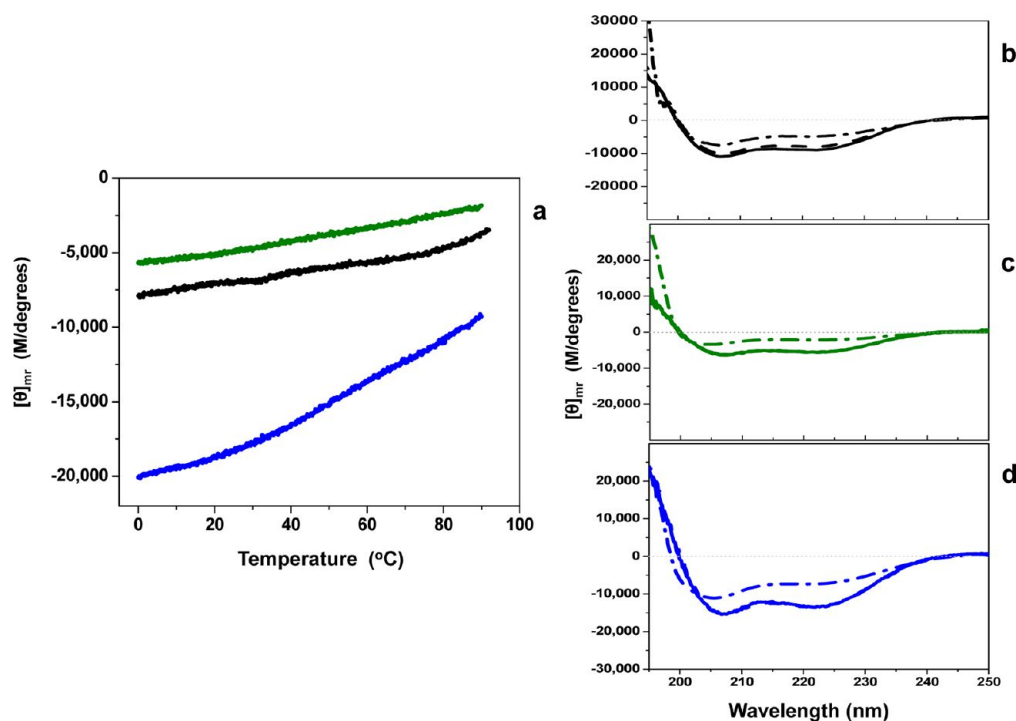


Figure 4. Relative thermal stability of *H. sapiens* centrins by CD analysis. (a) Thermal dependence of the helical regions among centrins Hscen1 (black), Hscen2 (green), and Hscen3 (blue). (b–d) Overlay of spectra of far-UV CD at 5 (—), 25 (---), and 85 °C (— · —) within the spectral region of 195–250 nm for (b) Hscen1, (c) Hscen2, and (d) Hscen3. The greatest helical content is observed for Hscen3. Also, the relative stabilities established for the thermal dependence of the helical regions for these centrins are in good agreement with the DSC results.

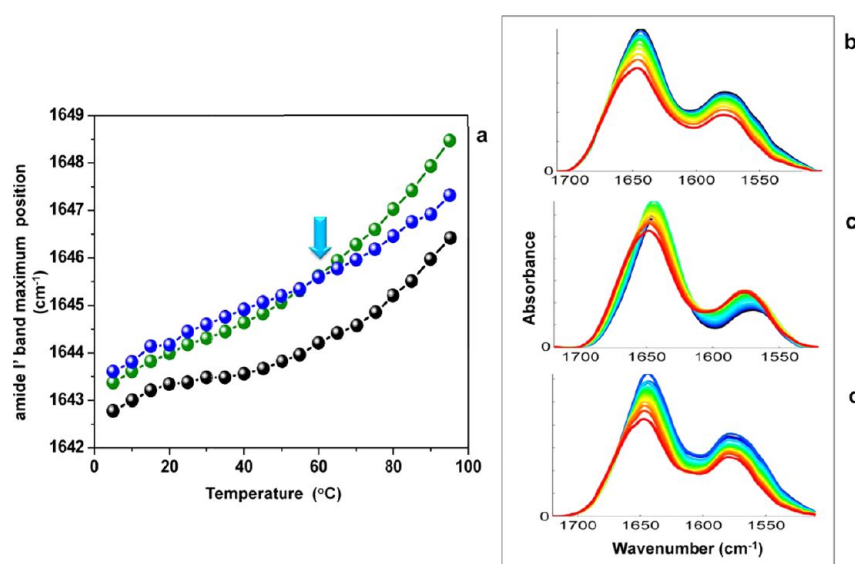


Figure 5. FT-IR thermal dependence study for H → D exchanged wild-type centrin within the temperature range of 5–95 °C. (a) Thermal dependence plots for *Hscen1* (black), *Hscen2* (green), and *Hscen3* (blue). The plot shows the amide I' band maximum as a function of temperature, which is sensitive to all of the backbone $\nu(\text{C}=\text{O})$ vibrational modes of the protein. The vertical dashed line denotes the first temperature range for all centrin. Also highlighted with the light blue arrow is the temperature (60 °C) at which the *Hscen3* curve begins to depart from *Hscen2*. (b–d) FT-IR spectral overlay of wild-type centrin amide I' and side chain bands in the spectral region of 1710–1500 cm^{-1} within the temperature range of 5–95 °C: (b) *Hscen1*, (c) *Hscen2*, and (d) *Hscen3*.

Table 2. Summary of the Peak Assignments for Backbone Vibrational Modes within the Amide I' Band (1710–1600 cm^{-1}) As Determined by the Synchronous and Asynchronous Plots

peak assignment	average peak position (cm^{-1})	<i>Hscen1</i> ^a peak position (cm^{-1})		<i>Hscen2</i> ^a peak position (cm^{-1})		<i>Hscen3</i> ^a peak position (cm^{-1})		
		5–35 °C	40–95 °C	5–35 °C	40–95 °C	5–35 °C	40–60 °C	60–90 °C
CaBS loop ^b	1682.8	1686.0	1687.5	1680.0	1683.7	1684.3	1682.4	1675.7
loops	1668.1	1668.8	1666.0	1666.7	1672.5	1671.4	1668.6	1662.8
π -helix	1653.1	1653.7	1652.0	<u>1653.4</u>	1653.7	1654.2	1654.8	1649.9
α -helix	1643.9	1642.5	<u>1642.0</u>	1643.4	1646.2	1641.4	1645.6	<u>1646.1</u>
β -sheet	1631.2	1635.0	1626.0	1636.7	<u>1638.7</u>	<u>1626.3</u>	<u>1627.2</u>	1628.7

^aUnderlined peak positions represent the greatest intensity change (i.e., the level of perturbation or flexibility) for the auto peaks within the synchronous plot. ^bThe calcium binding site (CaBS) loop would ordinarily be assigned as a β -turn, but for relevant structural discussions related to the well-known EF-hand motif, we have used the nomenclature associated with these calcium binding proteins.

loss of weak interactions between the helix–loop–helix motifs that are destabilized due to the EF-hand transitions between open and closed conformations arises from the lack of divalent cation coordination with the respective oxygens within the calcium binding loop. Interestingly, the ΔH_D determined for *Crcen* is twice the value for *Hscen3* and *Hscen2*, suggesting the destabilizing effect on the EF-hand motif is similar, although for *Hscen3* only one CaBS (III) located on the C-terminal domain has a lower affinity, while for *Hscen2*, two CaBS in the N-terminal domain have lower affinity. For *Hscen1*, both N- and C-terminal domains contain one CaBS (II and III) with lower affinity, and thus, the ΔH_D is roughly one-half that of *Hscen3*.

Relative Stability of the Helical Component of Centrin. CD experiments were performed to determine the helical content of the human centrin under identical buffer conditions. In addition, CD was used to investigate the extent to which the helical components were being destabilized during thermal denaturation. A relationship consistent with that established by the DSC endotherms was confirmed, as shown in Figure 4a. The mean residue molar ellipticity at 222 nm was monitored as a function of temperature. In addition, the crossover point, random coil, and helical mean residue molar

ellipticity for each centrin were determined at 25 °C and are summarized in Table S1 of the Supporting Information. Also shown are the spectral overlays for each human centrin at 5, 25, and 85 °C (Figure 4b–d). All are consistent with exhibition of an isodichroic point, suggesting these proteins undergo a series of conformational changes that do not involve a typical helix-to-random coil transition, but rather a different type of transition, which is discussed below.⁴⁴ Therefore, a simple two-state model cannot be assumed for these proteins, thus preventing further analysis.

Vibrational Spectroscopy. The FT-IR thermal dependence plot and the spectral overlay of the amide I' and side chain bands within the spectral region of 1710–1500 cm^{-1} are shown in Figure 5 for fully H → D exchanged *Hscen1*, *Hscen2*, and *Hscen3*. The amide I' band (1710–1600 cm^{-1}) is composed primarily of peptide bond frequencies [$\nu(\text{C}=\text{O})$] that are sensitive to conformational changes within proteins. In general, the amide I'/side chain band ratio varies slightly among human centrin, suggesting differences in the calcium binding state.⁴⁰ The side chain band (1600–1500 cm^{-1}) is composed of arginine guanidinium [$\nu_a(\text{N}-\text{D})$ and $\nu_s(\text{N}-\text{D})$], aspartate, and glutamate [$\nu_{a-s}(\text{COO}^-)$] side chain vibrational modes^{47,48}

located near or within the CaBS of these proteins and thus serving as probes of these sites.^{32,40,49,50} Furthermore, the carboxylate asymmetric stretching vibrations within the aspartate and glutamate residues are sensitive to the coordination state with calcium, such that when calcium is unbound because of the thermal perturbation, there is a peak shift toward higher wavenumbers (Table 2). This fact allows the identification of the lower- and higher-affinity CaBS.

The position of the peak maximum of the amide I' band as a function of temperature is used to generate the thermal dependence plots for all three human centrin as shown in Figure 5a. *Hscen1* and *Hscen2* share similar curve shapes but different relative stabilities, in good agreement with both CD thermal dependence and the DSC endotherms, in which *Hscen1* is more stable than *Hscen2*. Also, *Hscen1* and *Hscen2* both reveal a pretransition at ~20 °C. Meanwhile, *Hscen3* reveals characteristics similar to those of *Hscen2* at low temperatures, yet above 60 °C, the curve departs from that of *Hscen2*, suggesting differences in backbone dynamics, presumably because of the similarities in the calcium binding affinities it shares with both proteins (*Hscen2* and *Hscen1*). To improve our understanding of the relationship between the backbone dynamics and the calcium binding sites, 2D IR correlation analysis was performed, the results of which are discussed below.

Band Assignments. Contributing backbone vibrational modes within the FT-IR spectral overlay and 2D IR correlation analysis are summarized below for the amide I' band (1710–1600 cm^{-1}) and side chain band (1600–1500 cm^{-1}). In general, all spectral data sets are arranged in columns, and the similar plot types are arranged in rows to facilitate comparison and analysis (Figures 6–8). The band assignments were made using the asynchronous plot for which the highest spectral resolution was obtained and extrapolated to the synchronous and baseline-corrected spectral overlay for each data set to validate the assignment. A summary of the actual band positions for these centrin samples is shown in Tables 2 and 3. The average of the actual peak positions for the backbone vibrational modes determined for each asynchronous plot was used to facilitate interpretation and comparison. Several spectral overlays within the range of 1710–1500 cm^{-1} for *Hscen1*, *Hscen2*, and *Hscen3* are shown in Figures 6–8, respectively. The acquired spectra were separated into spectral data sets based on specific temperature ranges (step analysis) to ascertain the thermally induced molecular changes that occurred in the independent terminal domains of these related calcium binding proteins.⁴¹ The first temperature range studied for *Hscen1* and *Hscen2* was the 5–35 °C range (pretransition) shown in panels A, C, and E of Figures 6 and 7. The second temperature range for *Hscen1* and *Hscen2* used was the 40–95 °C range shown in panels B, D, and F of Figures 6 and 7. Meanwhile, for *Hscen3*, which exhibited a different thermal dependence plot (Figure 8) compared to those *Hscen2* and *Hscen1*, the spectral data set was separated into three steps: 5–35 °C (Figure 8A,D,G), 40–60 °C (Figure 8B,E,H), and 65–90 °C (Figure 8C,F,I). The band assignments presented below have been validated and are consistent with the available X-ray structural information, previous studies with *C. reinhardtii* centrin, and the correlations observed within the asynchronous plots during the thermal perturbation.^{30–33,40–42} The amide I' band comprises several backbone vibrational modes (Table 2) for the β -turn (1682.8 cm^{-1}), which will be considered as a CaBS loop, because it is associated with the short antiparallel β -

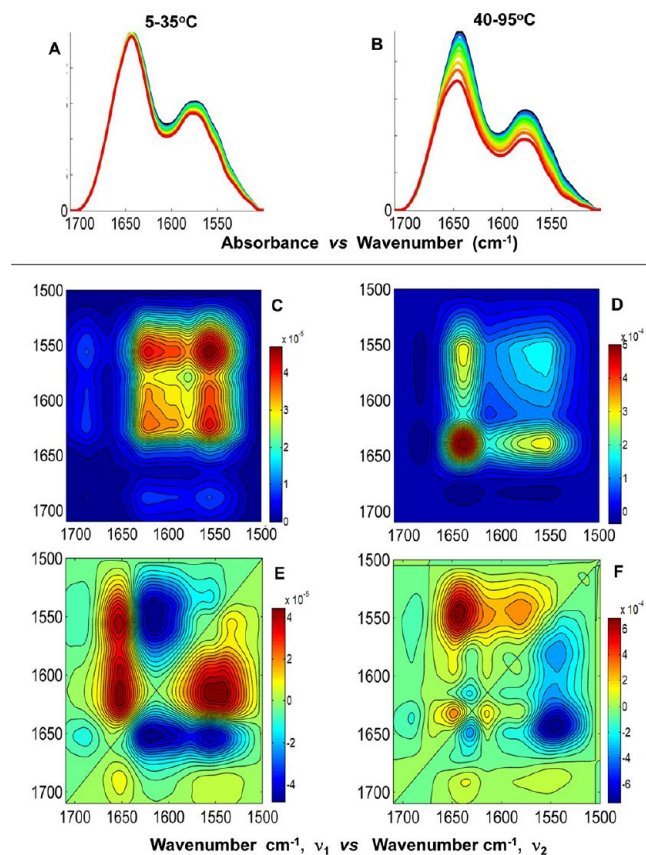


Figure 6. 2D IR correlation spectroscopy step analysis of *Hscen1* (WT) within the spectral region of 1710–1500 cm^{-1} . (A and B) FT-IR spectral overlays of the amide I' and side chain bands corresponding to the temperature ranges of 5–35 and 40–95 °C, respectively. (C and D) Synchronous plots and (E and F) asynchronous plots corresponding to the temperature ranges of 5–35 and 40–95 °C, respectively.

sheet segments located within the CaBS;^{32,40,42} the loops (1668.1 cm^{-1}), also termed the hinge region between the two EF-hand motifs; the π -helix (1653.1 cm^{-1}), located at the C-terminal end of all human centrin; the α -helical regions (1643.9 cm^{-1}); and the β -sheets (1631.2 cm^{-1}). The side chain modes are summarized in Table 3 and include the arginine guanidinium N–D antisymmetric and symmetric stretching modes consistent with our previous studies,^{40,41} and the aspartates and glutamates, which are located mainly within the CaBS and contain carboxylate stretching modes [$\nu_{\text{as}}(\text{COO}^-)$] sensitive to coordination with a divalent cation.^{40,49,50} Lower wavenumbers for the aspartate and glutamate carboxylate stretching modes are associated with the bound calcium state.⁴⁰ As calcium is released, first from the low-affinity CaBS and then from the high-affinity CaBS, the peak positions shift to higher wavenumbers characteristic of the unbound (apo) state.

2D IR Correlation Spectroscopy. This technique enhances the resolution of the spectral region of interest via the synchronous and asynchronous plots and provides the order of events that occur during the thermal perturbation. The auto-peaks found on the diagonal of the synchronous plots show changes in intensity that occur in the spectral region of interest, and the cross-peaks relate the auto-peaks that are in phase with one another. Meanwhile, the asynchronous plots are composed exclusively of cross-peaks that change in intensity out of phase from one another. According to Noda's rules, the

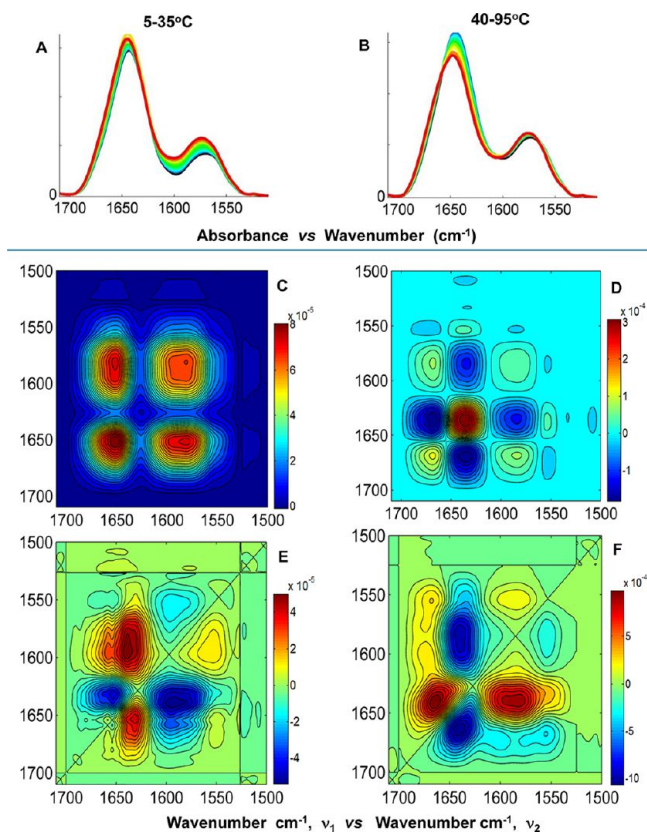


Figure 7. 2D IR correlation spectroscopy step analysis of *Hscen2* (WT) within the spectral region of 1710–1500 cm^{-1} . (A and B) FT-IR spectral overlays of the amide I' and side chain bands corresponding to the temperature ranges of 5–35 and 40–95 $^{\circ}\text{C}$, respectively. (C and D) Synchronous plots and (E and F) asynchronous plots corresponding to the temperature ranges of 5–35 and 40–95 $^{\circ}\text{C}$, respectively.

phase information in the asynchronous plot is used to ascertain the order of events when the synchronous plot is composed of positive cross-peaks. The order of events is reversed when the corresponding cross-peak in the synchronous plot is negative.^{38,39}

Similarities in Conformational Dynamics among Human Centrin. The auto-peaks in the synchronous plot comprise the overall intensity changes (i.e., the magnitude of change) associated with the backbone and side chain modes due to the temperature perturbation as indicated in Tables 2 and 3. Small changes in intensity are equivalent to smaller molecular fluctuations. These intensity changes reflect the thermal instability of the protein, and therefore, a comparative analysis of the overall effect of temperature on each protein can be conducted, providing the molecular similarities associated with the regions of greatest flexibility among the centrin. For *Hscen1* (WT) in the temperature range of 5–35 $^{\circ}\text{C}$, the aspartates (1561.4 cm^{-1}), presumably of the low-affinity CaBS (II and III), had the greatest perturbation, while in the temperature range of 40–95 $^{\circ}\text{C}$, the α -helical regions (1643.9 cm^{-1}) had the greatest flexibility. For *Hscen2* (WT) in the temperature range of 5–35 $^{\circ}\text{C}$, the π -helix (1653.1 cm^{-1}) located at the C-terminal end of the protein had the greatest flexibility, while in the temperature range of 40–95 $^{\circ}\text{C}$, it was the short antiparallel β -sheet segments (1631.2 cm^{-1}) located within the CaBS. This suggested that certain backbone vibrational modes are more flexible in *Hscen2*, which exhibited

the lowest thermal transition temperature. For *Hscen3* (WT) in the temperature ranges of 5–35 and 40–60 $^{\circ}\text{C}$, the short antiparallel β -sheet segments (1631.2 cm^{-1}) were located within the CaBS, while the largest intensity change within the temperature range of 65–90 $^{\circ}\text{C}$ was assigned to the α -helical regions (1643.9 cm^{-1}) of *Hscen3*. The greatest perturbation observed for *Hscen3* (WT) in the temperature ranges of 5–35 and 40–60 $^{\circ}\text{C}$ was in the β -sheet, consistent with that of *Hscen2* (WT) at 40–95 $^{\circ}\text{C}$. The greatest perturbation observed for *Hscen3* (WT) in the temperature range of 65–90 $^{\circ}\text{C}$ was in the α -helical regions, consistent with that of *Hscen1* (WT) at high temperatures. Thus, the similarities in the regions of the protein with greatest molecular flexibility between these centrin proteins were established.

Differences in Conformational and Side Chain Dynamics among Human Centrin. The sequential order of events describes the molecular behavior of these human centrin within the defined temperature ranges to allow for the evaluation of the relative stability of these proteins as shown in Figures 9–11 and summarized in Tables S2–S4 of the Supporting Information. For *Hscen1* (WT), similar conformational dynamics were observed in both temperature ranges (5–35 and 40–95 $^{\circ}\text{C}$), which is consistent with both N- and C-terminal domains containing one EF-hand motif in the open conformation, while the other EF-hand motif is in the closed conformation. The vibrational modes perturbed in the temperature range of 5–35 $^{\circ}\text{C}$ are summarized in Figure 9a. This molecular behavior presumably involving the CaBS II and III describes the pretransition observed for *Hscen1* (WT). At higher temperatures leading up to thermal denaturation (40–95 $^{\circ}\text{C}$) shown in Figure 9b, similar backbone vibrational modes are perturbed, while the side chains are presumably within the higher-affinity CaBS (I and IV) within *Hscen1* (Figure 1).

For *Hscen2* (WT), the protein behaves more like two independent domains, with the C-terminal domain being more stable than the N-terminal domain. The N-terminal domain is composed of EF-hands in the closed conformation, allowing more flexibility in the β -sheets and helical regions, while the C-terminal domain has both EF-hands in the open conformation causing the π -helix to be perturbed first in the higher temperature range. A summary of the molecular events that occurred in the temperature range of 5–35 $^{\circ}\text{C}$ is shown in Figure 10a. This sequential order of molecular events describes the pretransition of *Hscen2* (WT) at higher temperatures leading to denaturation (40–95 $^{\circ}\text{C}$), which are summarized in Figure 10b. These final events of the sequence are consistent with the EF-hand motif undergoing the transition from the open to the closed conformation, leading to thermal unfolding.

For *Hscen3* (WT), the C-terminal domain initially had conformational dynamics similar to those of *Hscen1* in which one EF-hand motif is in the open conformation while the other is in the closed conformation. Thermal destabilization begins to occur in the temperature range of 5–35 $^{\circ}\text{C}$ (Figure 11a) within the loop hinge of the C-terminal end (1668.1 cm^{-1}). The second temperature range analyzed for *Hscen3* was the 40–60 $^{\circ}\text{C}$ range (Figure 11b), in which the molecular behavior was similar to that of *Hscen2* where both EF-hand motifs within the N-terminal domain are in the open conformation. The third temperature range analyzed for *Hscen3* was the 65–90 $^{\circ}\text{C}$ range (Figure 11c). The conformational dynamics are unique in that the initial sequential order of events was different from that of *Hscen2* and *Hscen1*. This is consistent with the thermal dependence plot shown in Figure 4, in which the *Hscen3* curve

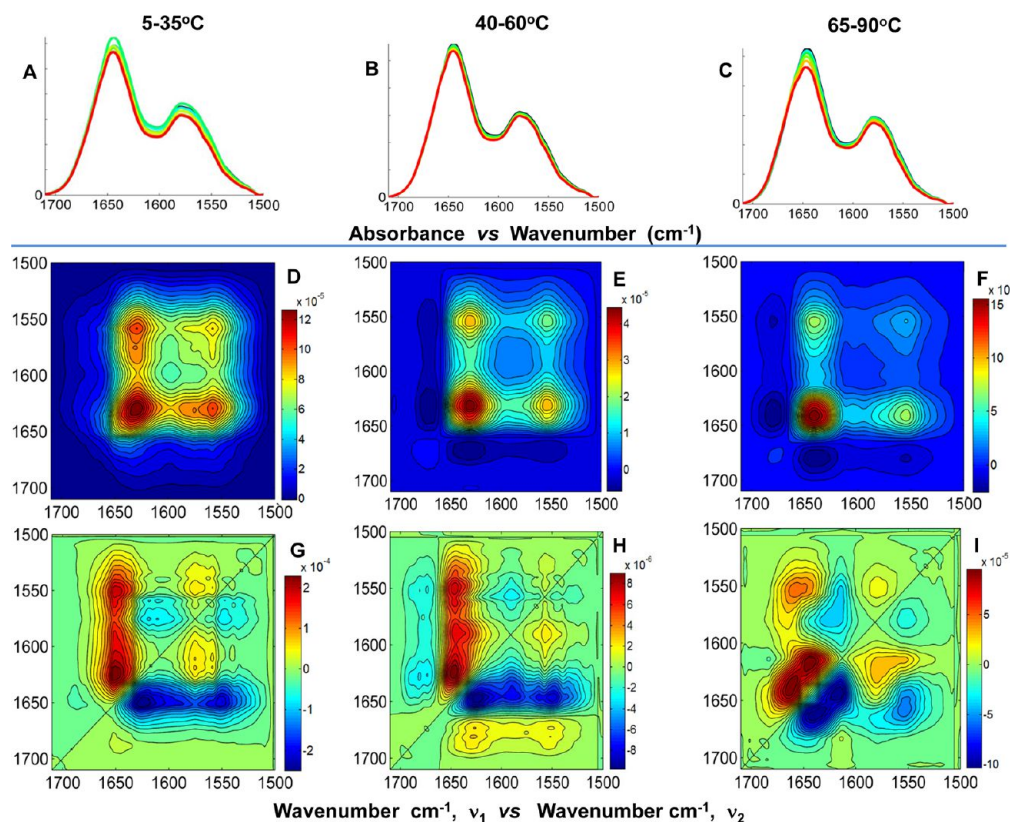


Figure 8. 2D IR correlation spectroscopy step analysis of Hscen3 (WT) within the spectral region of 1710–1500 cm^{-1} . (A–C) FT-IR spectral overlays of the amide I' and side chain bands corresponding to the temperature ranges of 5–35, 40–60, and 65–90 $^{\circ}\text{C}$, respectively. (D–F) Synchronous plots and (G–I) asynchronous plots corresponding to the temperature ranges of 5–35, 40–60, and 65–90 $^{\circ}\text{C}$, respectively.

Table 3. Summary of the Peak Assignments for the Side Chain Vibrational Modes within the Side Chain Band (1600–1500 cm^{-1}) As Determined by the Synchronous and Asynchronous Plots

peak assignment ^b	stretching vibrational mode	Hscen1 ^a peak position (cm^{-1})		Hscen2 peak position (cm^{-1})		Hscen3 peak position (cm^{-1})		
		5–35 $^{\circ}\text{C}^c$	40–95 $^{\circ}\text{C}^d$	5–35 $^{\circ}\text{C}^c$	40–95 $^{\circ}\text{C}^d$	5–35 $^{\circ}\text{C}^c$	40–60 $^{\circ}\text{C}^c$	60–90 $^{\circ}\text{C}^d$
arginine	guanidinium $\nu_s(\text{N-D})$	1608.7	1610.0	1603.4	1602.8	1604.2	1608.8	1613.3
arginine	guanidinium $\nu_s(\text{N-D})$	1578.7	1586.2	1591.8	1597.5	1581.3	1585.8	1581.3
aspartate	$\nu_s(\text{COO}^-)$	<u>1561.4</u>	1566.0	1572.5	1575.0	1560.5	1562.8	1564.1
glutamate	$\nu_s(\text{COO}^-)$	1539.0	1548.0	1546.8	1552.5	1546.9	1551.3	1555.6

^aThe underlined peak position represents the greatest intensity change for the auto peaks within the synchronous plot. ^bHscen1 and Hscen2 contain a single Tyr residue, and Hscen3 contains two Tyr residues, observed at 1517 cm^{-1} , which will not be discussed in this work. ^cAspartate and glutamate peak positions are characteristic of the bound state, presumably in the lower-affinity CaBS.⁴¹ ^dAspartate and glutamate peak positions are characteristic of the unbound (apo) state within the high-affinity CaBS. The loss of calcium binding occurs because of the high-temperature perturbation as a prerequisite step to thermal unfolding.

deviates from the Hscen2 and Hscen1 curves in having a different slope and therefore can be explained at the molecular level as summarized in Figure 11c.

DISCUSSION

The differences we have observed in the molecular behavior of human centrins are governed by the affinity for Ca^{2+} within the different CaBS. In general, the lower-affinity CaBS were perturbed first, leading to the differences in the molecular behavior among the EF-hand motifs and in turn affecting the terminal EF-hand domain where these lower-affinity sites are located. Similarly, as the temperature was increased, the higher-affinity CaBS were perturbed, losing the coordination with the divalent cation and causing the molecular flexibility associated with the transition from the open to the closed conformation

within the EF-hand motifs. These differences in molecular behavior are important factors that can be used to explain the interaction with a wide variety of biological targets and the diverse roles centrins are observed to have.

When the binding of calcium stabilizes the EF-hand domain in the open conformation, it allows for increased surface area and exposes side chains that would normally be buried for potential interaction with their biological target. It is this interface and the residues that comprise it that are selective for a particular target; therefore, a lower-affinity Ca^{2+} site would be less likely to accommodate a biological target. This observation may also explain the relative dependence on calcium affinity exhibited by different centrin biological targets. The hinge loop region is also very important because of the biochemical differences dictated by the residue composition.

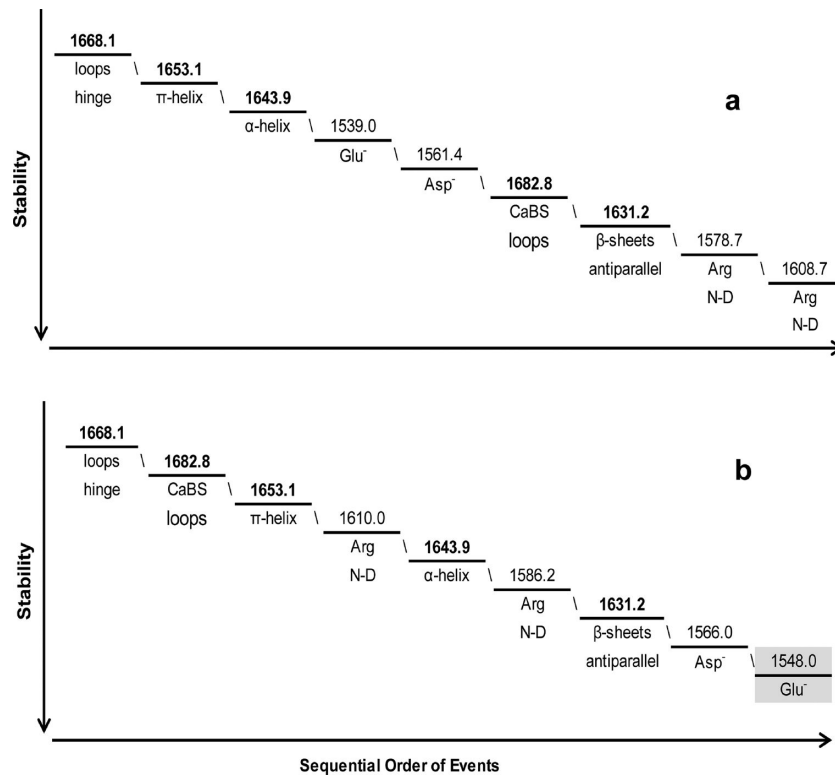


Figure 9. Sequential order of molecular events for *Hscen1* (WT) in the temperature ranges of (a) 5–35 and (b) 40–95 °C. The lowest temperature range includes the Glu⁻ and Asp⁻ side chain perturbations that are presumably associated with the lower-affinity CaBS (II and III) as shown in Figure 1.^{32,40} The most stable vibrational mode (40–95 °C) was determined to be the glutamates within the high-affinity CaBS (I and IV) as highlighted in panel b.

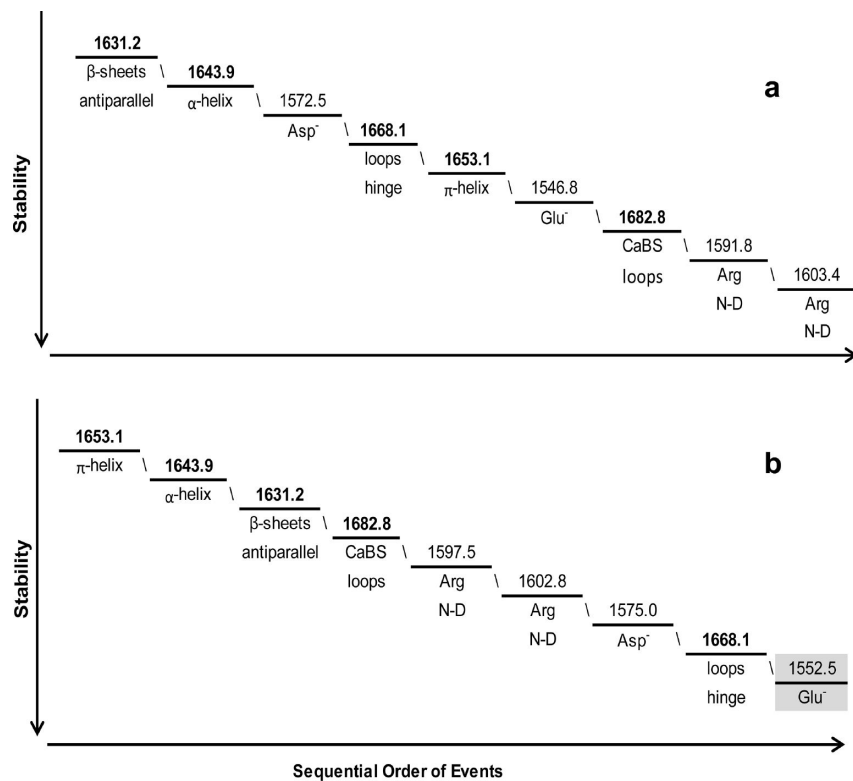


Figure 10. Sequential order of molecular events for *Hscen2* (WT) for the temperature ranges of (a) 5–35 and (b) 40–95 °C. The most stable vibrational mode (40–95 °C) was determined to be the glutamates within the high-affinity CaBS (III and IV)^{30,31} as highlighted in panel b.

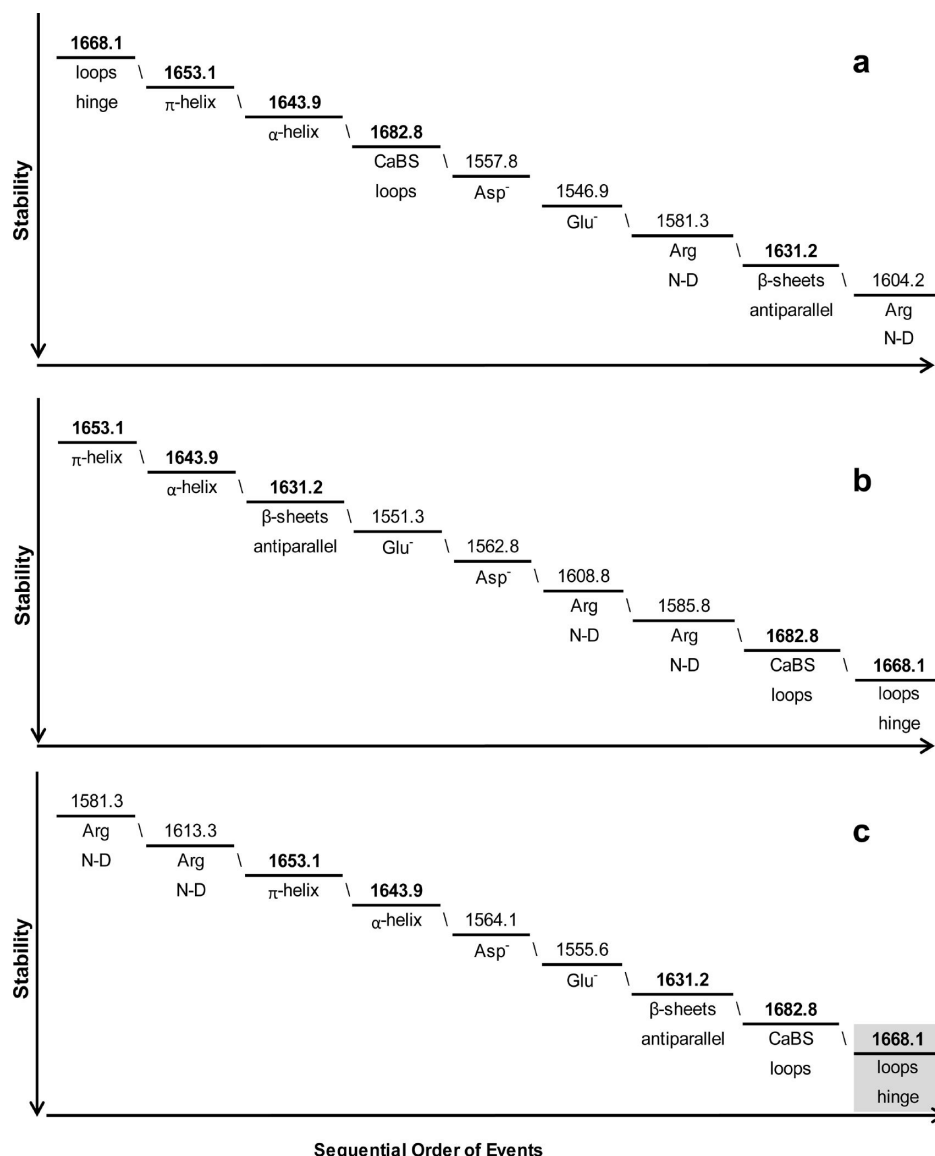


Figure 11. Sequential order of molecular events for Hscen3 (WT) for the temperature ranges of (a) 5–35, (b) 40–60, and (c) 65–90 °C. In the low temperature range of 5–35 °C, the low-affinity CaBS (III) is perturbed, while the most stable vibrational mode (65–90 °C) was determined to be the loops within the EF-hand domains that contained the high-affinity CaBS as highlighted in panel c.

Another important factor is the intrinsic molecular flexibility dictated by the sequence composition within the EF-hand motif, which causes the differences in dynamics within these structural domains. It is these differences in molecular flexibility that affect the overall complex formation and its stability. This is especially true when one considers *C. reinhardtii* centrin, which, although all of its sites are bound to calcium, is the most stable of the centrans. Crce’s level of molecular flexibility within the C-terminal domain and hinge loop residue composition provide the optimal conditions for binding a model peptide, melittin.³² This Crce–melittin complex, like the Hscen2–XPC complex, adopts an extended conformation, while other centrin complexes, among them the centrin–Sfi1p complex, adopt a different wrap-around conformation requiring the flexibility of the tethered helix.^{31,32,51} It is, in part, this flexibility that allows centrin to have multiple biological targets and is a hub within the interactome.

Other potential implications may be inferred at the cellular level for centrin in general. In the work by Winey’s group using

Tetrahymena thermophila, selective site-directed mutants, specifically Asp⁻ for Ala at the X position of different CaBS, were constructed to cause a decrease in calcium affinity at a particular site.²⁹ The cellular outcomes observed were misorientation of the basal body and changes in its stability. If we consider the differences in molecular flexibility observed in *H. sapiens* centrans caused by their differences in calcium affinity, then it is feasible to envision the effect on the molecular flexibility of the *Tetrahymena thermophila* centrin (centrin 1), which might then affect formation of the centrin–target complex and, in turn, the structure of the basal body within this model organism. Further investigation is warranted, and we plan to pursue the study of different centrin–biological target complexes in the near future.

In summary, 2D IR correlation spectroscopy has proven to be an excellent technique for the evaluation of the relative stability of centrans. These novel 2D IR results were in good agreement with the more traditional DSC and CD data and provided a detailed molecular explanation for the differences in

stability among highly related centrin. We anticipate that this technique will also be suitable for the evaluation of recombinant protein therapeutics for the evaluation of their relative stability and viability.

■ ASSOCIATED CONTENT

● Supporting Information

Amino acid sequence alignment of *H. sapiens* and *C. reinhardtii* centrin (Figure S1), DSC thermograms within the temperature range of 10–130 °C (Figure S2), summary of far-UV CD comparative analysis of *H. sapiens* centrin (Table S1), summary of the sequential order of events for *Hscen1* (WT) (Table S2), summary of sequential order of events for *Hscen2* (WT) (Table S3), and summary of sequential order of events for *Hscen3* (WT) (Table S4). This material is available free of charge via the Internet at <http://pubs.acs.org>.

■ AUTHOR INFORMATION

Corresponding Author

*University of Puerto Rico, Mayagüez Campus, Mayagüez, PR 00681-9019. Telephone: (787) 832-4040, ext. 2302. Fax: (787) 265-3849. E-mail: belinda@hpcf.upr.edu or belinda.pastrana@gmail.com.

Funding

This project is supported by National Institutes of Health SCORE Grant SO6GM08103 (B.P.-R.), the Henry Dreyfus Teacher Scholar Award (B.P.-R.), the Alfred P. Sloan Foundation (A.R.N.), and the University of Puerto Rico.

Notes

The authors declare no competing financial interest.

■ ACKNOWLEDGMENTS

We thank Drs. Elmar Schiebel (Peterson Institute for Cancer Research) and John Kilmartin (University of Cambridge) for providing the centrin cDNA, Dr. Juan Carlos Martinez-Cruzado (University of Puerto Rico, Mayagüez, PR) for performing the cDNA sequencing of the centrin recombinants, Dr. Michael Berne (Tufts University, Medford, MA) for performing the partial amino acid sequencing of the centrin proteins, and Dr. Melissa Stauffer (Scientific Editing Solutions, Walworth, WI) for editing the manuscript.

■ ABBREVIATIONS

2D IR, two-dimensional infrared; DSC, differential scanning calorimetry; CD, circular dichroism; *Hscen1*, centrin 1; *Hscen2*, centrin 2; *Hscen3*, centrin 3; *Hscen4*, centrin 4; MTOC, microtubule organizing center; *Crcen*, *C. reinhardtii* centrin; CaBS, calcium binding sites; FT-IR, Fourier transform infrared.

■ REFERENCES

- (1) Hartman, H., and Federov, A. (2002) The origin of the eukaryotic cell: A genomic investigation. *Proc. Natl. Acad. Sci. U.S.A.* 99, 1420–1425.
- (2) Salisbury, J. L. (2007) A mechanistic view on the evolutionary origin for centrin-based control of centriole duplication. *J. Cell. Physiol.* 213, 420–428.
- (3) Giessl, A., Trojan, P., Pulvermuller, A., and Wolfrum, U. (2004) Centrin, Potential Regulators of Transducin Translocation in Photoreceptor Cells. In *Photoreceptor cell biology and inherited retinal degenerations* (Williams, D. S., Ed.) pp 195–215, World Scientific, Singapore.
- (4) Laoukili, J., Perret, E., Middendorp, S., Houcine, O., Guennou, C., Marano, F., Bornens, M., and Tournier, F. (2000) Differential

expression and cellular distribution of centrin isoforms during human ciliated cell differentiation in vitro. *J. Cell Sci.* 113, 1355–1364.

(5) Gavet, O., Alvarez, C., Gaspar, P., and Bornens, M. (2003) Centrin4p, a novel mammalian centrin specifically expressed in ciliated cells. *Mol. Biol. Cell* 14, 1818–1834.

(6) Araki, M., Masutani, C., Takemura, M., Uchida, A., Sugasawa, K., Kondoh, J., Ohkuma, Y., and Hanaoka, F. (2001) Centrosome group centrin2/caltractin1 is part of the xeroderma pigmentosum group C complex that initiates global genome nucleotide excision repair. *J. Biol. Chem.* 276, 18665–18672.

(7) Nishi, R., Okuda, Y., Watanabe, E., Mori, T., Iwai, S., Masutani, C., Sugasawa, K., and Hanaoka, F. (2005) Centrin 2 stimulates nucleotide excision repair by interacting with xerodermapigmentosum group C protein. *Mol. Cell. Biol.* 25, 5664–5674.

(8) Resendes, K. K., Rasala, B. A., and Forbes, D. J. (2008) Centrin 2 Localizes to the Vertebrate Nuclear Pore and Plays a Role in mRNA and Protein Export. *Mol. Cell. Biol.* 28, 1755–1769.

(9) Manandhar, G., Simerly, C., Salisbury, J. L., and Schatten, G. (1997) Centrosome reduction during mouse spermiogenesis: Centriole and centrin degeneration. *Mol. Biol. Cell* 8 (Suppl.), 56a.

(10) Palermo, G. D., Joris, H., Devroey, P., and Van Steirteghem, A. C. (1992) Pregnancies after intra cytoplasmic sperm injection of single spermatozoon into an oocyte. *Lancet* 340, 17–18.

(11) Pearson, C. C., Giddings, T. H., and Winey, M. (2009) Basal body components exhibit differential protein dynamics during nascent basal body assembly. *Mol. Biol. Cell* 20, 904–914.

(12) Salisbury, J. L., Suino, K., Busby, R., and Springett, M. (2002) Centrin-2 is required for centriole duplication in mammalian cell. *Curr. Biol.* 12, 1287–1292.

(13) Nigg, E. A. (2007) Centrosome duplication: Of rules and licenses. *Trends Cell Biol.* 17, 215–221.

(14) Lingle, W. L., Barrett, S. L., Negrón, V., D'Assoro, A., Whitehead, C. M., and Salisbury, J. L. (2001) Chromosomal instability and loss of tissue differentiation in breast tumors correlate with independent aspects of centrosome amplification. *Mol. Biol. Cell* 12, 175A.

(15) Lingle, W. L., Barrett, S. L., Negrón, V. C., D'Assoro, A. B., Boeneman, K., Liu, W., Whitehead, C. M., Reynolds, C., and Salisbury, J. L. (2002) Centrosome amplification drives chromosomal instability in breast tumor development. *Proc. Natl. Acad. Sci. U.S.A.* 99, 1978–1983.

(16) Dawe, H. R., Farr, H., and Gull, K. (2007) Centriole/basal body morphogenesis and migration during ciliogenesis in animal cells. *J. Cell Sci.* 120, 7–15.

(17) Hoyer-Fender, S. (2010) Centriole maturation and transformation. *Semin. Cell Dev. Biol.* 21, 142–147.

(18) Bandano, J. L., Mitsuma, N., Beales, P. L., and Katsanis, N. (2006) The Ciliopathies: An emerging class of human genetic disorders. *Annu. Rev. Genomics Hum. Genet.* 7, 125–148.

(19) Hildebrandt, F., Benzing, T., and Katsanis, N. (2011) Mechanism of Disease Ciliopathies. *N. Engl. J. Med.* 364, 1533–1543.

(20) Ostrowski, L. E., Dutcher, S. K., and Lo, C. W. (2011) Cilia and models for studying structure and function. *Proc. Am. Thorac. Soc.* 8, 423–429.

(21) Bettencourt-Dias, M., Hildebrandt, F., Pellman, D., Woods, G., and Godinho, S. A. (2011) Centrosomes and cilia in human disease. *Trends Genet.* 27, 307–315.

(22) Lee, J. E., and Gleeson, J. G. (2011) A systems-biology approach to understanding the ciliopathy disorders. *Genome Med.* 1–9.

(23) Novariano, G., Akizu, N., and Gleeson, J. G. (2011) Modeling human disease in humans: The ciliopathies. *Cell* 147, 7079.

(24) Zaki, M. S., Sattar, S., Massoudi, R. A., and Gleeson, J. G. (2011) Co-Occurrence of distinct ciliopathy diseases in single families suggests genetic modifiers. *Am. J. Med. Genet., Part A* 9999, 1–8.

(25) Marshall, J. D., Maffei, P., Collin, G. B., and Naggert, J. K. (2011) Alström Syndrome: Genetics and Clinical Overview. *Curr. Genomics* 12, 225–235.

(26) Bergmann, C. (2011) Educational paper: Ciliopathies. *Eur. J. Pediatr.* 171, 1285–1300.

- (27) Delaval, B., Covassin, L., Lawson, N. D., and Doxsey, S. (2011) Centrin depletion causes cyst formation and other ciliopathy-related phenotypes in zebrafish. *Cell Cycle* 10, 3964–3972.
- (28) Koblenz, B., Schoppmeier, J., Grunow, A., and Lechtreck, K. F. (2003) Centrin deficiency in *Chlamydomonas* causes defects in basal body replication, segregation and maturation. *J. Cell Sci.* 116, 2635–2646.
- (29) Vonderfecht, T., Stemm-Wolf, A. J., Hendershott, M., Giddings, T. H., Jr., Meehl, J. B., and Winey, M. (2011) The two domains of centrin have distinct basal body functions in *Tetrahymena*. *Mol. Biol. Cell* 22, 2221–2234.
- (30) Gifford, J. L., Walsh, M. P., and Vogel, H. (2007) Structures and metal-ion-binding properties of the Ca²⁺-binding helix-loop-helix EF-hand motifs. *Biochem. J.* 405, 199–221.
- (31) Thompson, J. R., Ryan, Z. C., Salisbury, J. L., and Kumar, R. (2006) The structure of the human centrin 2-xeroderma pigmentosum group C protein complex. *J. Biol. Chem.* 281, 18746–18752.
- (32) Sosa, L. D. V., Alfaro, E., Santiago, J., Narváez, D., Rosado, M. C., Rodríguez, A., Gómez, A. M., Schreiter, E., and Pastrana-Rios, B. (2011) The Structure, Molecular Dynamics, and Energetics of Centrin-Melittin Complex. *Proteins: Struct., Funct., Bioinf.* 79, 3132–3143.
- (33) Nakayama, S., and Kretsinger, R. H. (1998) Classification and evolution of EF-hand proteins. *BioMetals* 11, 277–295.
- (34) Veeraraghavan, S., Fagan, P. A., Hu, H., Lee, V., Harper, J. F., Huang, B., and Chazin, W. J. (2002) Structural independence of the two EF-hand domains of caltractin. *J. Biol. Chem.* 277, 28564–28571.
- (35) Weber, C., Lee, V. D., Chazin, W. J., and Huang, B. (1994) High-level expression in *Escherichia coli* and characterization of the EF-hand calcium-binding protein caltractin. *J. Biol. Chem.* 269, 15795–15802.
- (36) Makhatadze, G. I. (2001) Measuring protein thermostability by differential scanning calorimetry. *Curr. Protoc. Protein Sci.*, 7.9.1–7.9.14.
- (37) Berova, N., Nakanishi, K., and Woody, R. W., Eds. (2000) *Circular dichroism, principles and applications*, 2nd ed., pp 912, John Wiley and Sons, New York.
- (38) Noda, I. (2004) Advances in two-dimensional correlation spectroscopy. *Vib. Spectrosc.* 36, 143–165.
- (39) Noda, I. (2008) Recent advancement in the field of two-dimensional correlation spectroscopy. *J. Mol. Struct.* 883, 2–26.
- (40) Pastrana-Rios, B., Ocaña, W., Rios, M., Vargas, G. L., Ysa, G., Poynter, G., Tapia, J., and Salisbury, J. L. (2002) Centrin: Its secondary structure in the presence and absence of cations. *Biochemistry* 41, 6911–6919.
- (41) Pastrana-Rios, B. (2001) Mechanism of Unfolding of a Model Helical Peptide. *Biochemistry* 40, 9074–9081.
- (42) Sanoguet-Carrero, Z., Campbell, M., Ramos, S., Seda, C., and Pastrana-Rios, B. (2006) Effects of phosphorylation in *Chlamydomonas* centrin Ser 167. *Calcium Binding Proteins* 1, 108–114.
- (43) Lafitte, D., Tsvetkov, P. O., Devred, F., Toci, R., Barras, F., Briand, C., Makarov, A. A., and Haiech, J. (2002) Cation binding mode of fully oxidized calmodulin explained by the unfolding of the apostate. *Biochim. Biophys. Acta* 1600, 105–110.
- (44) Sorensen, B. R., and Shea, M. A. (1998) Interactions between domains of Apo Calmodulin Alter Calcium Binding and Stability. *Biochemistry* 37, 4244–4253.
- (45) Fabian, H., and Mantele, W. (2002) Infrared Spectroscopy of Proteins. In *Encyclopedia of Analytical Chemistry*, pp 1–24, John Wiley & Sons Ltd., New York.
- (46) Arrondo, J. L. R., Muga, A., Castresana, J., and Goñi, F. M. (1993) Quantitative Studies of the Structure of Proteins in Solution by Fourier-transform Infrared Spectroscopy. *Prog. Biophys. Mol. Biol.* 59, 23–56.
- (47) Chirgadze, Y. N., Fedoroy, V., and Trushina, N. P. (1975) Estimation of amino acid residue side-chain absorption in the infrared spectra of protein solutions in heavy water. *Biopolymers* 14, 679–694.
- (48) Venyaminov, S. Y., and Kalnin, N. N. (1990) Quantitative IR spectrophotometry of peptide compounds in water (H₂O) solutions. 1. Spectral parameters of amino-acid residue absorption-bands. *Biopolymers* 30, 1243–1257.
- (49) Mizuguchi, M., Nara, M., Kawano, K., and Nitta, K. (1997) FT-IR study of the Ca²⁺-binding to bovine α -lactalbumin. Relationships between the type of coordination and characteristics of the bands due to the Asp⁻ COO⁻ groups in the Ca²⁺-binding site. *Eur. J. Biochem.* 250, 72–76.
- (50) Nara, M., Morii, H., and Tanokura, M. (2012) Coordination to divalent cations by calcium-binding proteins studied by FT-IR spectroscopy. *Biochim. Biophys. Acta*, 10.1016/j.bbamem.2012.11.025.
- (51) Li, S., Sandercock, A. M., Conduit, P., Robinson, C. V., Williams, R. L., and Kilmartin, J. V. (2006) Structural role of Sfi1p-centrin filaments in budding yeast spindle pole body duplication. *J. Cell Biol.* 173, 867–877.